Surface creep along the Longitudinal Valley fault, Taiwan from InSAR measurements

Leslie Hsu[1] and Roland Bürgmann[1]

Received 12 September 2005; revised 6 February 2006; accepted 14 February 2006; published 25 March 2006.

[1] We use interferometric synthetic aperture radar (InSAR) analysis in eastern Taiwan to study reverse creep on the Longitudinal Valley fault (LVF). A stack of the three highest-quality image pairs spanning 1997–2000 shows sharp range change offsets along the eastern side of the Longitudinal Valley, suggesting 11–35 mm/yr of surface creep between 23 and 23.4°N. No shallow slip was observed along the northern or southern ends of the valley, nor on mapped fault traces on the western edge of the valley. The width of the zone of deformation varied, suggesting distributed shear in shallow sediments above the creeping fault in some places. The InSAR results support the view that although surface creep is rapid in certain locations, significant portions of the LVF are locked and thus represent a substantial seismic hazard. **Citation:** Hsu, L., and R. Bürgmann (2006), Surface creep along the Longitudinal Valley fault, Taiwan from InSAR measurements, *Geophys. Res. Lett.*, *33*, L06312, doi:10.1029/2005GL024624.

1. Introduction

[2] Some of the most rapid tectonic uplift rates in the world occur in Taiwan, where the Eastern Coastal Range is being thrust up along the east-dipping Longitudinal Valley fault (LVF). The LVF accounts for ~30 mm/yr of present-day shortening [*Yu and Kuo*, 2001], or 30% of the total plate convergence [*Angelier et al.*, 2000]. The fault zone displays both creeping and locked segments and has produced moderate to large earthquakes [e.g., *Cheng et al.*, 1996; *Kuochen et al.*, 2004]. Active shallow creep has been monitored by creepmeters [*Lee et al.*, 2003, 2005], GPS [*Yu and Kuo*, 2001; *Chen et al.*, 2004a], leveling [e.g., *Yu and Liu*, 1989], and repeat surveying of manmade structures [*Angelier et al.*, 2000]. This study presents interferometric synthetic aperture radar (InSAR) results from the Longitudinal Valley, which complement existing measurements, providing greater spatial coverage of the surface deformation along the LVF. We focus on establishing the distribution and magnitude of near-fault deformation associated with shallow localized fault creep.

2. Geometry and Kinematics of the Longitudinal Valley Fault

[3] Relocated seismicity south of 23.5°N suggests a 45–60° east-dipping fault near the surface whose dip shallows with depth and connects with a décollement at ~20–40 km depth [*Kuochen et al.*, 2004; *Rau et al.*, 2005]. The seismicity indicates that the fault geometry in the northern half of the LVF is more complicated, with no obvious fault plane extending to the surface [*Kuochen et al.*, 2004]. A left-lateral strike-slip component is inferred along the fault zone that may be partitioned between sub-parallel thrust and strike-slip fault segments along portions of the fault [*Angelier et al.*, 2000; *Hu et al.*, 2001]. There is still debate about how much regional deformation is accommodated by the LVF, a possible Central Valley fault to the west, and offshore faults to the east [e.g., *Bos et al.*, 2003; *Shyu et al.*, 2005].

[4] Along-strike, the existing deformation measurements suggest highest creep rates near Chihshang and decreasing rates toward the northern and southern tips (Figure 1). Shallow creep rates inferred from GPS velocities vary longitudinally [*Chen et al.*, 2004a] and may reach up to 40 mm/yr in the southern section [*Hsu et al.*, 2003]. The local creep rate of the fault near Chihshang as derived from near-fault data is ~26–28 mm/yr in a N40°W direction [*Angelier et al.*, 2000; *Chen et al.*, 2004a]. However, uncertainties remain regarding the spatial extent and degree of localization of along-strike and cross-strike surface deformation.

[5] Creep rates along the LVF appear to be variable in time, at both seasonal and decadal scales. *Lee et al.* [2003, 2005] found creep rates two to three times higher during the wet period (Apr.-Oct.) than during the dry season (Nov. to Mar.). Decadal trends in repeat ground-surveying of man-made structures suggest a 25% decrease in rate from the 1980s to the 1990s [*Angelier et al.*, 2000], possibly continuing up to the M_w = 6.8 Chengkung earthquake of 10 December 2003 [*Lee et al.*, 2005]. Millennial uplift rates derived from Holocene river incision into terraces suggest a 20 mm/yr uplift rate (J. B. H. Shyu, manuscript in preparation, 2006). Some geodetically determined slip rates appear to exceed the sparse geologic estimates and active slip is generally variable in time. Creep rate estimates determined from the 1997–2000 InSAR data should thus only be directly compared to other measurements obtained during that time period.

3. InSAR Processing and Results

[6] We use synthetic aperture radar data obtained by the European Space Agency's ERS-1 and 2 satellites. Along descending track 461, we selected 11 scenes covering the southern Longitudinal Valley and 6 scenes covering the northern valley, acquired between 23 June 1993 and 11 May 2002 (Table S1).[1] We processed the data with the Repeat

[1]Department of Earth and Planetary Science, University of California, Berkeley, California, USA.

0094-8276/06/2005GL024624$05.00

[1]Auxiliary material is available at ftp://ftp.agu.org/apend/gl/2005gl024624.

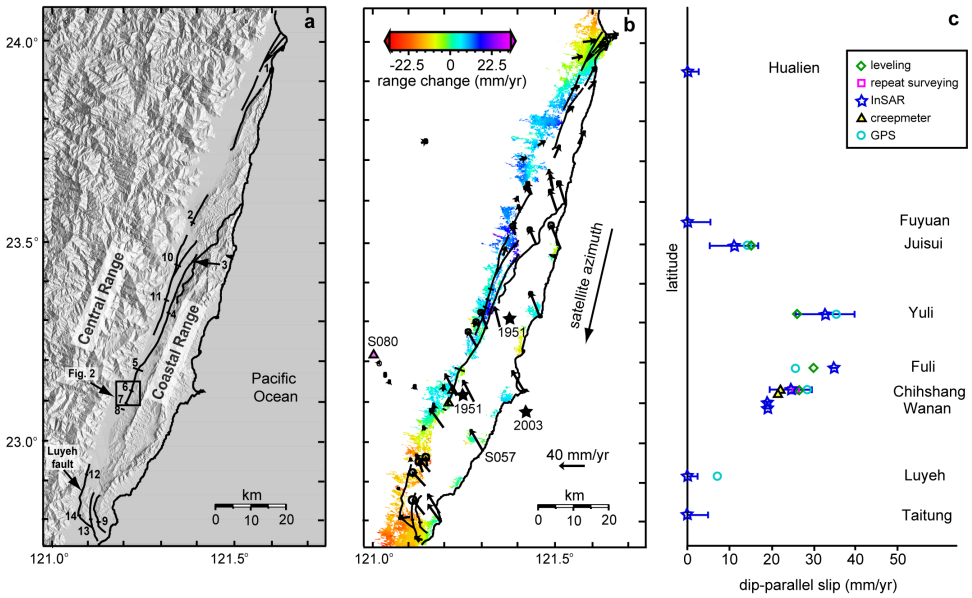

Figure 1. (a) DEM of eastern Taiwan with fault lines [*Lin et al.*, 2000] and range-change profile locations (see Table 1). (b) Range change per year in the Longitudinal Valley shown by interferometric stack of three pairs (see Figure S1). Shown are creepmeters (yellow triangles), GPS velocities (black arrows, relative to S080 purple triangle) from *Yu and Kuo* [2001] with 95% confidence ellipses. (c) Comparison of dip-parallel slip as measured by leveling [*Yu and Liu*, 1989], repeat surveying [*Angelier et al.*, 2000], InSAR (this study), creepmeter [*Lee et al.*, 2003], and GPS [*Yu and Kuo*, 2001; *Chen et al.*, 2004a]. Uncertainties for the creepmeter, GPS, leveling, and repeat survey values are under 2 mm/yr, within the size of the plotted symbol. The uncertainties of the InSAR estimates are obtained from the RMS scatter on either side of the fault trace.

Orbit Interferometry Package (ROI-PAC) developed at JPL, supplemented with the SNAPHU unwrapper [*Chen and Zebker*, 2001]. Twelve interferometric pairs were generated, all with orbital baseline differences less than 100 meters (Figure S1). Topographic effects were removed with a 40-m DEM. During processing, orbital baselines were re-estimated to minimize the phase gradient across the scene. However, this process also may remove a real regional gradient due to interseismic deformation. For example, near Chihshang, 3D velocities of a row of GPS stations from the coast (station S057) to the Central Range (S080) correspond to a predicted range-change rate of 38 ± 5 mm/yr over 40 km. About 34 mm/yr of the offset occurs within the valley, the other 4 mm/yr occurs in the Coastal and Central Ranges. Nonetheless, the removal of a regional range-change gradient will have a negligible effect on surface deformation measured on short (1–2 km) profiles across the fault. We do not attempt to infer deformation at depth from far-field interferometry.

[7] Obtaining coherent and reliable InSAR measurements in this area is challenging, due to the nature of the land-cover, atmospheric errors, and other possible confounding signals such as groundwater-related movement. The land cover in the valley is mostly agricultural or urban with some river beds and the surrounding ranges are heavily vegetated. Accordingly, the coherence of the interferometric pairs is greatest in the valley and degrades quickly as elevation and vegetation density increases. Since the fault usually borders topography, large coherent patches on both sides of the mapped fault are intermittent. To create an interferogram with reduced atmospheric error and a longer time span, we formed a stack from the three pairs with the largest coherent areas, covering a total duration of 1260 days (Figure 1b). The stacking process averages the phase gradient while eliminating data pixels without coherence in all three pairs (Figure S2).

4. Surface Deformation and Creep

[8] The data were analyzed by examining 400-m-wide swath profiles of range change rates across selected areas of the mapped fault trace (Figures 1a and S4). We chose 14 profile locations based on coherence of the InSAR data and relationship to the mapped fault trace. Because the satellite track (S13°W) is sub-parallel to the trace of the fault (S20°W), vertical and fault-perpendicular slip components dominantly map into the range-change measurement. We projected the range change detected by the satellite into the fault-perpendicular dip-slip direction, assuming a near-surface fault dip angle of 45° and a satellite look angle of 23° from vertical (Figure S3 and Table S2).

[9] At each location, we evaluate the magnitude of the range change rate and the width of the zone of range change (Table 1). Because of possible errors from atmospheric interference and other InSAR uncertainties, no single interferogram is taken as proof of a deformation pattern. Thus, in addition to considering the stacked interferogram, we examine profiles across the 11 individual interferograms. Only if four or more pairs show a consistent range-change offset, do we consider the creep estimate as robust. We find that where we observe offsets in the fault-crossing profiles, the offset is found in all pairs that span less than 385 days, and most pairs that span 525 days. Visual inspection of the wrapped interferograms confirms that temporal decorrela-

Table 1. Dip-Parallel Slip on the LVF[a]

Label	Location	Range Change, mm/yr	Dip-Slip, mm/yr	Offset Width, m
		East		
1	Hualien	0 ± 2	0 ± 3	-
2	Fuyuan	0 ± 2	0 ± 6	-
3	Juisui	4 ± 2	11 ± 6	300–400
4	Yuli	12 ± 3[b]	32 ± 7	200–400
5	Fuli	13 ± 1	35 ± 2	1000–1400
6	Chihshang	9 ± 2	24 ± 5	100–200
7	Wanan North	7 ± 1	19 ± 2	400–500
8	Wanan South	7 ± 1[c]	19 ± 2	250–400
9	Taitung	0 ± 2	0 ± 5	-
		West		
10	Wuhi Tableland	0 ± 3	0– ± 7	-
11	W Yuli	0 ± 1	0 ± 2	-
12	Luyeh	0 ± 1	0 ± 3	-
13	W Taitung	0 ± 1	0 ± 1	-
14	W Taitung 2	0 ± 1	0 ± 3	-

[a]Dip-parallel slip is calculated for a 45° east-dipping fault with thrust vergence in the N70°W direction, the uncertainty of the slip rate is estimated from the RMS scatter of the data surrounding the deformation zone. The width of deformation is the distance over which the InSAR offset occurs.
[b]Value derived from pairs 970517–980502 and 970726–980815 only.
[c]Value derived from pairs 970726–980815 and 980815–000122 only.

tion of the longer time-span pairs lowers coherence to such a degree that SNAPHU's unwrapping algorithm often infers a flat signal (see Figure S4).

[10] On the east side of the valley, we observe a large offset in range change between 23 and 23.4°N at our locations Chihshang, Fuli, and Yuli (Figure 1). Smaller offsets are found south and north of this segment at the locations Wanan South, Wanan North, and Juisui. The width of the deformation zone is narrowest (~150 m) at Chihshang (Figures 2 and 3a) and widest (~1200 m) at Fuli (Figure 3b). No appreciable offset was observed at the northern or southern ends of the valley at Taitung, Fuyuan or Hualien, nor on profiles across mapped fault traces [e.g., *Shyu et al.*, 2005] on the west side of the valley bounded by the Central Range. However, we point out that the coherent InSAR data do not sufficiently cover all mapped faults in the valley (e.g., Figure 1b), so we cannot evaluate some regions.

[11] The interferometric pairs span time periods between 1993 and 2000, with durations between four and thirty months. The slip-rate estimates from the interferometric stack at Chihshang (covering 1997–2000) are similar to those measured by *Angelier et al.* [1997] during 1982–1994. This suggests that the creep rate at this location has been relatively constant over the past two decades. The seasonal pattern that was detected by *Lee et al.* [2003] cannot be tested with our data set, since the timing of our pairs does not emphasize the seasonal differences. However, the range of slip measurements between different pairs could be attributed to variation in seasonal make-up of the pairs.

5. Discussion and Conclusion

[12] Figure 1c (data in Table S2) summarizes the InSAR results together with previous field measurements. InSAR suggests that the steadily creeping section terminates shortly north of Juisui and south of Wanan. Whereas GPS indicates creep continuing south between Wanan and Taitung, the InSAR data spanning the fault may have been too sparse to detect this. Also, motion in the strike-slip direction is not detected by the ERS descending satellite orientation, so areas with dominantly strike-slip motion would appear inactive. Confounding signals from atmospheric vapor and groundwater-related subsidence and rebound could be reduced with additional data that allow for more detailed investigation of seasonal effects.

[13] There have been several historical earthquakes of magnitude >6.0 on the creeping Chihshang segment, including the two 1951 Taitung (M_w = 6.2 and 7.0) and 2003 Chengkung (M_w = 6.8) earthquakes (Figure 1b). *Cheng et al.* [1996] note that meter-scale scarps were produced at the surface by the 1951 event between about 23.05 and 23.6°N, overlapping with the present-day area of highest creep rates. For the 2003 event located near Chihshang, *Chen et al.* [2004b] found coseismic vertical GPS offsets measuring over 20 cm and an additional 5 cm postseismic uplift over four months. This shows that even segments creeping at a high rate can have large strain-releasing events. Possibly, the pre-2003 creep rates measured on the Chihshang segment were postseismic transients from the 1951 events.

[14] Seismicity maps of eastern Taiwan indicate a conspicuous region with fewer earthquakes between 23.3 and 23.5°N [e.g., *Kuochen et al.*, 2004]. Directly south of this region is the well-imaged and rapidly creeping Chihshang segment. North of this region, the fault geometry is more complicated than a simple east-dipping thrust, and creep rates are not detectable. The seismically–quiet region itself has lower creep rates. In analogous creeping fault zones (e.g., the San Andreas in California) creeping fault segments are usually very microseismically active, and seismicity collapses into well defined planar features. Creeping faults

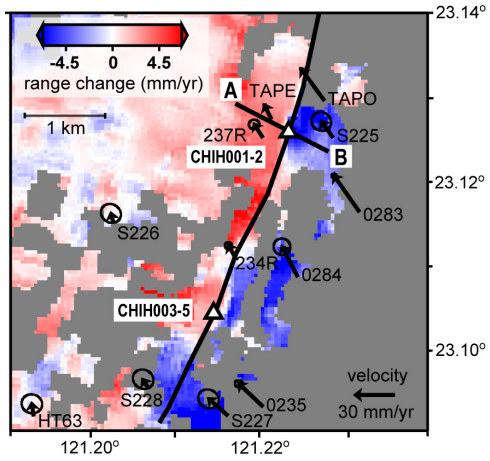

Figure 2. Interferometric stack of the Chihshang site (see Figure 1a for location), showing the mapped fault trace (black line) [*Lin et al.*, 2000], location of range change rate profile (400 meter-wide swath from A to B), creepmeters (white triangles) [*Lee et al.*, 2003], and GPS station velocities (black arrows with 95% confidence ellipses), with respect to station S080 in the Central Range [*Chen et al.*, 2004a].

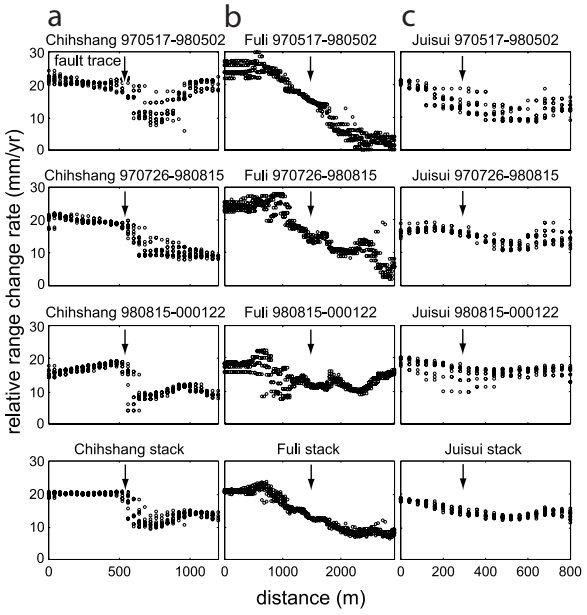

Figure 3. Profiles of range-change rate across the LVF for individual pairs and the composite stack. Swaths are 400 m wide with each point representing a 40 m by 40 m pixel. The dates are in YYMMDD format.

also tend to have repeating events among the on-fault seismicity. So, while not conclusive, the lack of seismicity, lack of well-defined planar features, and low creep rates between 23.3 and 23.5°N may suggest a more fully-locked section of the LVF. Continued monitoring of shallow slip along the LVF using InSAR will provide valuable information about the spatial and temporal evolution of aseismic slip and elastic strain accumulation along the fault. Such a monitoring effort will benefit from improved coherence of future L-band SAR systems and from a higher frequency of acquisitions.

[15] **Acknowledgments.** The authors would like to thank Ingrid Johanson and two anonymous reviewers for comments that improved the manuscript. Funding was provided by the Francis J. Turner Fellowship and the Taiwanese-American Foundation of Boston. ERS data were obtained through ESA Cat-1 project 1524. Berkeley Seismolab contribution 06–02.

References

Angelier, J., H. T. Chu, and J. C. Lee (1997), Shear concentration in a collision zone: Kinematics of the Chihshang Fault as revealed by outcrop-scale quantification of active faulting, Longitudinal Valley, eastern Taiwan, *Tectonophysics*, *274*, 117–143.

Angelier, J., H. T. Chu, J. C. Lee, and J. C. Hu (2000), Active faulting and earthquake hazard: The case study of the Chihshang Fault, Taiwan, *J. Geodyn.*, *29*, 151–185.

Bos, A. G., W. Spakman, and M. C. J. Nyst (2003), Surface deformation and tectonic setting of Taiwan inferred from a GPS velocity field, *J. Geophys. Res.*, *108*(B10), 2458, doi:10.1029/2002JB002336.

Chen, C. W., and H. A. Zebker (2001), Two-dimensional phase unwrapping with use of statistical models for cost functions in nonlinear optimization, *J. Opt. Soc. Am. A Opt. Image Sci.*, *18*, 338–351.

Chen, H. Y., S. B. Yu, Y. G. Chen, Y. R. Chuang, and H. Y. Hu (2004a), GPS measurements of near-fault crustal deformation in the south Longitudinal Valley, southeastern Taiwan, paper presented at 2004 International Symposium on GNSS/GPS, Univ. of N. S. W., Sydney, Australia.

Chen, H. Y., S. B. Yu, L. C. Kuo, and C. C. Liu (2004b), Coseismic and postseismic displacements of the 10 December 2003 (M_w 6. 5) Chengkung, eastern Taiwan, earthquake, paper presented at 2004 International Symposium on GNSS/GPS, Univ. of N. S. W., Sydney, Australia.

Cheng, S. N., Y. T. Yeh, and M. S. Yu (1996), The 1951 Taitung earthquake in Taiwan, *J. Geol. Soc. China*, *39*, 267–285.

Hsu, Y. J., M. Simons, S. B. Yu, L. C. Kuo, and H. Y. Chen (2003), A two-dimensional dislocation model for interseismic deformation of the Taiwan mountain belt, *Earth Planet. Sci. Lett.*, *211*, 287–294.

Hu, J. C., J. Angelier, C. Homberg, J. C. Lee, and H. T. Chu (2001), Three-dimensional modeling of the behavior of the oblique convergent boundary of southeast Taiwan: Friction and strain partitioning, *Tectonophysics*, *333*, 261–276.

Kuochen, H., Y. M. Wu, C. H. Chang, J. C. Hu, and W. S. Chen (2004), Relocation of eastern Taiwan earthquakes and tectonic implications, *Terr. Atmos. Ocean Sci.*, *15*, 645–666.

Lee, J. C., J. Angelier, H. T. Chu, J. C. Hu, F. S. Jeng, and R. J. Rau (2003), Active fault creep variations at Chihshang, Taiwan, revealed by creep meter monitoring, 1998–2001, *J. Geophys. Res.*, *108*(B11), 2528, doi:10.1029/2003JB002394.

Lee, J. C., J. Angelier, H. T. Chu, J. C. Hu, and F. S. Jeng (2005), Monitoring active fault creep as a tool in seismic hazard mitigation: Insights from creepmeter study at Chihshang, Taiwan, *C. R. Geosci.*, *337*, 1200–1207.

Lin, C. W., H. C. Huang, S. T. Lu, T. S. Shih, and W. J. Huang (Eds.) (2000), Active fault map of Taiwan, 2nd ed., scale 1:500,000, Cent. Geol. Surv., Taipai, Taiwan.

Rau, R. J., H. H. Chen, and K. E. Ching (2005), Seismogenesis of a crustal-scale creeping fault—The Chihshang fault of eastern Taiwan, *Geophys. Res. Abstr.*, *7*, Abstract 03837.

Shyu, J. B. H., K. Sieh, Y. G. Chen, and C. S. Liu (2005), Neotectonic architecture of Taiwan and its implications for future large earthquakes, *J. Geophys. Res.*, *110*, B08402, doi:10.1029/2004JB003251.

Yu, S. B., and L. C. Kuo (2001), Present-day crustal motion along the Longitudinal Valley fault, eastern Taiwan, *Tectonophysics*, *333*, 199–217.

Yu, S. B., and C. C. Liu (1989), Fault creep on the central segment of the Longitudinal Valley Fault, eastern Taiwan, *Proc. Geol. Soc. China*, *32*, 209–231.

R. Bürgmann and L. Hsu, Department of Earth and Planetary Science, University of California, Berkeley, Berkeley, CA 94720, USA. (lhsu@eps.berkeley.edu)

GEOPHYSICAL RESEARCH LETTERS, VOL. 33, L06312, doi:10.1029/2005GL024624, 2006

Surface creep along the Longitudinal Valley fault, Taiwan from InSAR measurements

Leslie Hsu and Roland Bürgmann

Auxiliary Materials

Figure S1. Dates and baseline difference for the 12 pairs. The interferograms in bold are used to form the stacks in Figures 1b, 2, and S2.

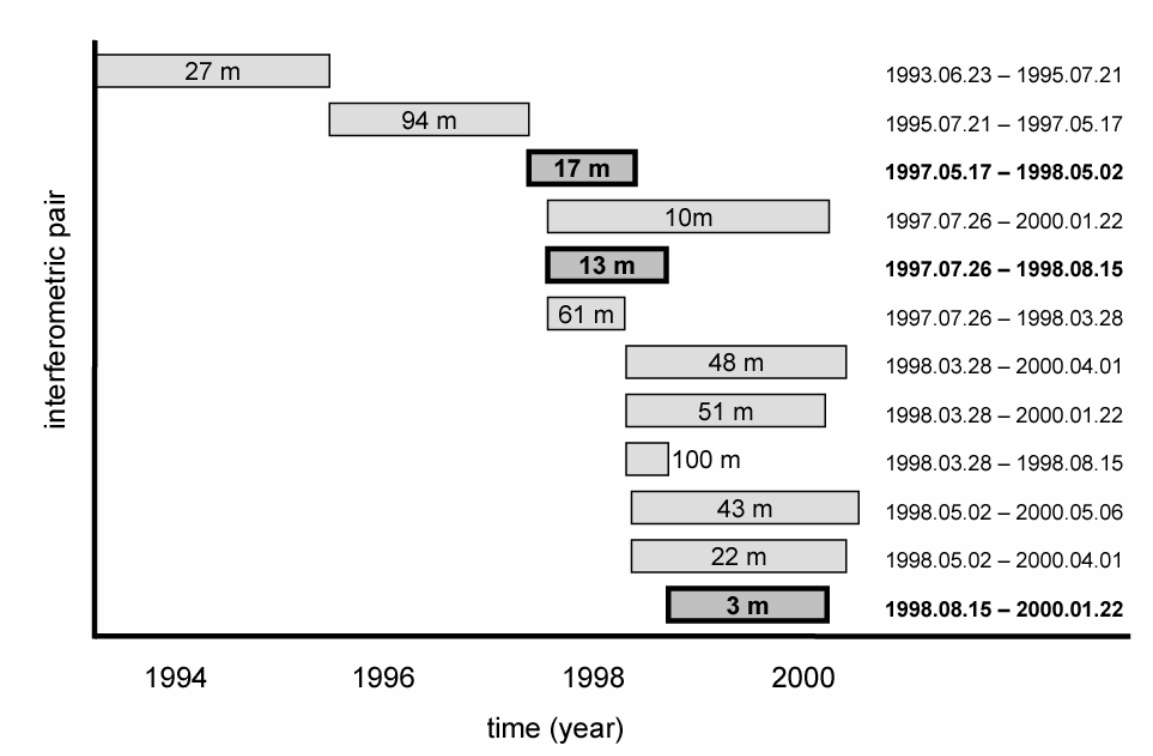

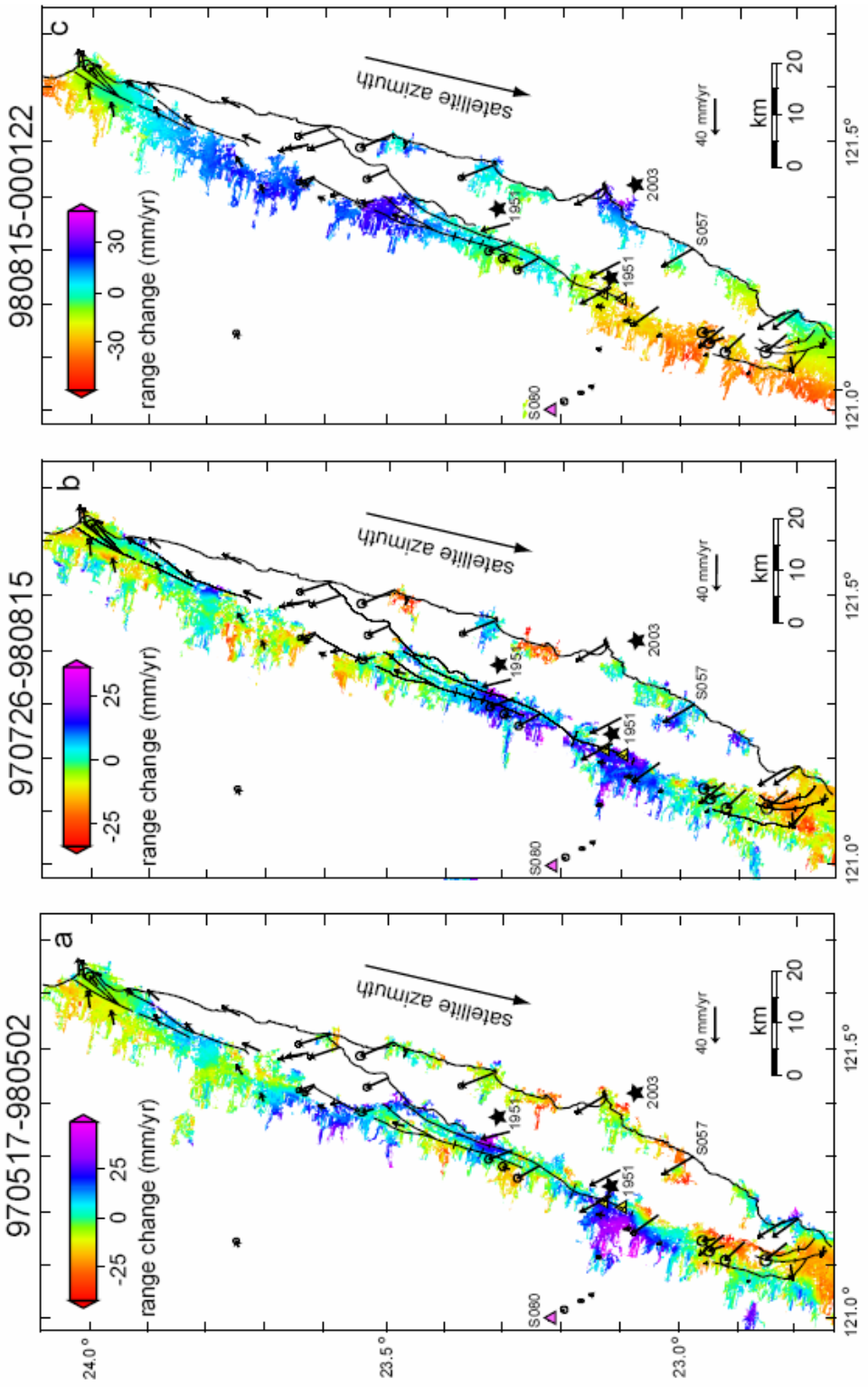

Figure S2. Individual interferograms from which the stack is made. The offset between the patches along the fault trace and the isolated patches on the east is not robustly determined and should be viewed with caution. Dates are in YYMMDD format.

Figure S3. Look angle diagram
The ERS satellites are right-looking with a look angle 23º from vertical. Westward thrusting on the LVF produces horizontal motions of the hanging wall block away from the ERS spacecraft (range increase) and uplift leading to range decrease. The satellite track (S13ºW) is sub-parallel to the strike of the LVF (S20ºW) and thus strike-slip motion does not project into the line of sight or range change vector. Fault dips > 23° produce a net range decrease of the hanging wall block (Coastal Range) with respect to the Longitudinal Valley. If the dip of the fault is 45° at the surface, then the range-change-rate difference across the fault is converted to slip rate by a factor of 1/(cosine 68°). Dip-parallel slip rates in Tables 1 and S2 are calculated assuming 45° dip.

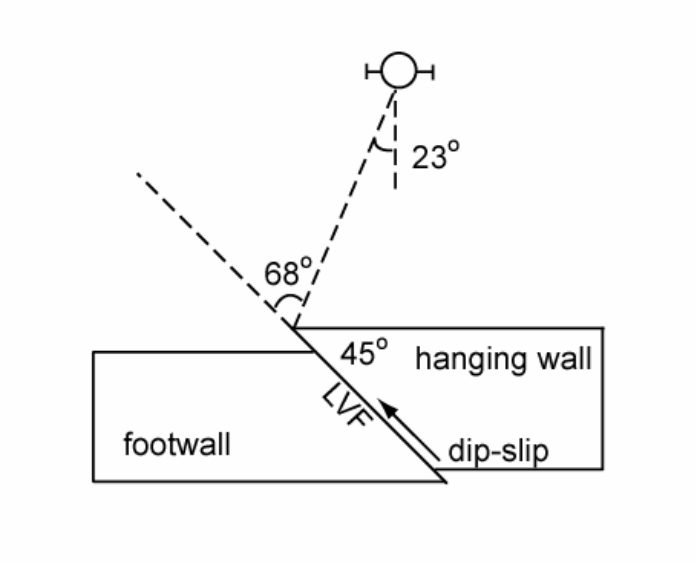

Table S1. Scenes selected for InSAR processing, descending track 461. Scenes were chosen with the criteria of a maximum perpendicular baseline of 94 meters and a maximum duration of 2.5 years. The 000511 scene did not process a coherent interferogram, likely because of Doppler shifts of the ERS-2 satellite during the Extra Back-up Mode period.

Mission	Date	Orbit	Frames
	YYYY.MM.DD		
ERS-1	1993.06.23	10125	3141
ERS-1	1995.07.21	20990	3141
ERS-2	1997.05.17	10836	3123, 3141
ERS-2	1997.07.26	11838	3123, 3141
ERS-2	1998.03.28	15345	3123, 3141
ERS-2	1998.05.02	15846	3123, 3141
ERS-2	1998.08.15	17349	3123, 3141
ERS-2	2000.01.22	24864	3123, 3141
ERS-2	2000.04.01	25866	3141
ERS-2	2000.05.06	26367	3141
ERS-2	2002.05.11	36888	3141

Table S2. Deformation measurements converted into dip-parallel slip. Dip-parallel slip is calculated for a 45º east-dipping fault with thrust vergence in the N70ºW direction.

Method	Reference	Period	Location	horizontal mm/yr	vertical mm/yr	range-change mm/yr	dip-parallel slip mm/yr
Leveling	Yu & Liu, 1989	1983-1988	Juisui		9.6		14
Leveling	Yu & Liu, 1989	1983-1988	Yuli		18		25
Leveling	Yu & Liu, 1989	1983-1988	Fuli		21		30
Leveling	Yu & Liu, 1989	1983-1988	Tapo		18.5		26
Surveying	Angelier et al., 1997	1982-1994	Chihshang	18			25
Surveying	Angelier et al., 2000	1990-1997	Chihshang	17			24
InSAR	This study	1997-2000	Juisui			4	11
InSAR	This study	1997-2000	Yuli			12	32
InSAR	This study	1997-2000	Fuli			13	35
InSAR	This study	1997-2000	Chihshang			9	24
InSAR	This study	1997-2000	Wanan 1			7	19
InSAR	This study	1997-2000	Wanan 2			7	19
InSAR	This study	1997-2000	Luyeh			0	0
Creepmeter	Lee et al., 2003	1998-2001	Tapo	16.2			23
Creepmeter	Lee et al., 2003	1998-2001	Chinyuan	15			21
GPS	Yu & Kuo, 2001	1996-1999	Juisui	10			14
GPS	Yu & Kuo, 2001	1985-1996	Yuli		24.4		35
GPS	Chen et al., 2004a	2000-2003	Fuli	17.5			25
GPS	Chen et al., 2004a	2000-2003	Chihshang	20			28
GPS	Yu & Kuo, 2001	1997-1999	Luyeh	14			20

Figure S4. Profiles of range change rate, all locations listed in Table 1 and shown in Figure 1. Arrows show the location of the mapped fault [Lin et al., 2000]. Date-pairs are listed in Figure S1 (YYMMDD). 980328-980815 is not shown because it had much more scatter in its range change points due to the short time duration. Stack 1 consists of 970517-980502, 970726-980815, and 980815-000122. Profile swaths are 400 meters wide with each point representing a 40 meter by 40 meter pixel. Blank plots indicate that there was no coherent signal in that location for that particular date-pair. Note that because of the geometry of the fault, upward thrust on the eastern side would be indicated by a decrease in range change toward the satellite. Therefore, from left to right, a downward step in range change indicates west-vergent thrusting on the LVF. Note that where we observe offsets in the fault-crossing profiles, the offset is found in all pairs that span less than 385 days (panels marked with **black stars**), and most pairs that span 525 days (panels marked with **open stars**). Visual inspection of the wrapped interferograms confirms that temporal decorrelation of the longer time-span pairs lowers coherence to such a degree that SNAPHU's unwrapping algorithm often infers a flat signal.

1. Hualien

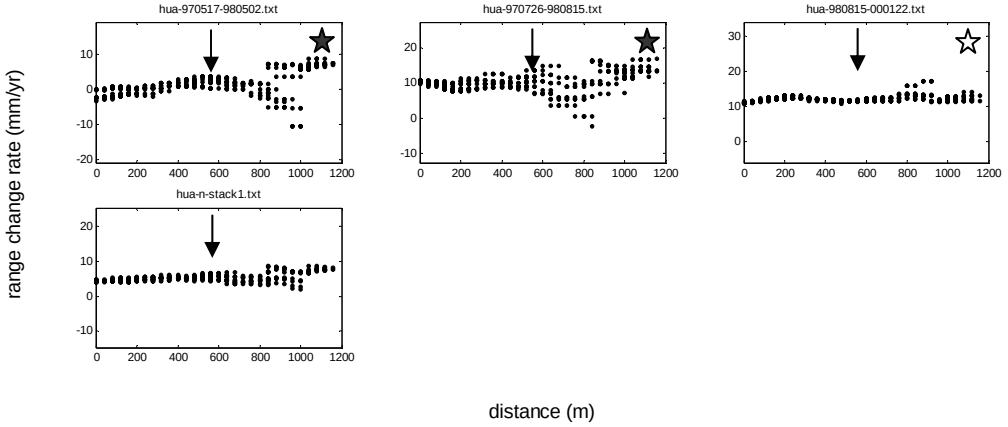

2. Fuyuan

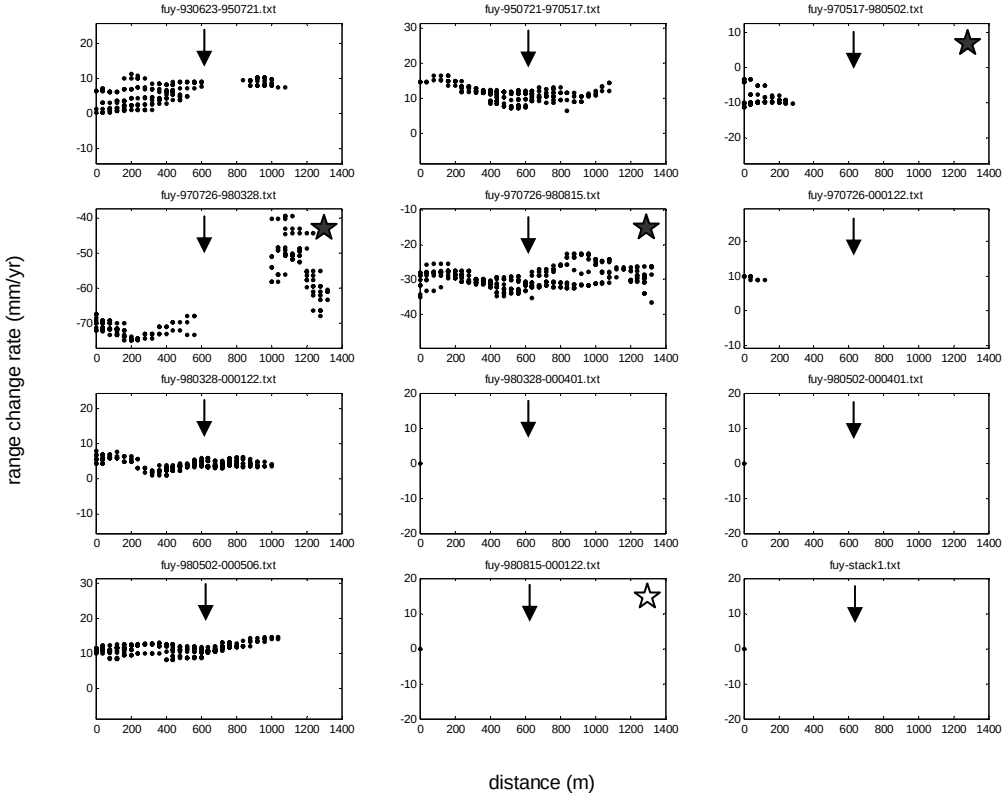

3. Juisui

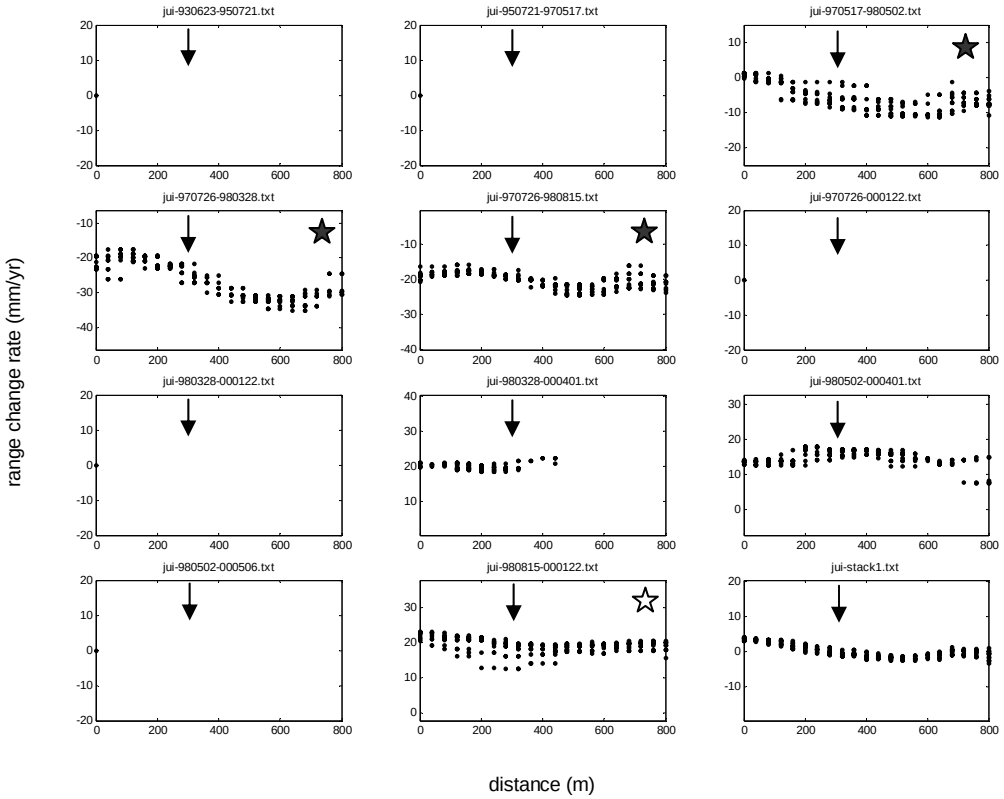

4. Yuli

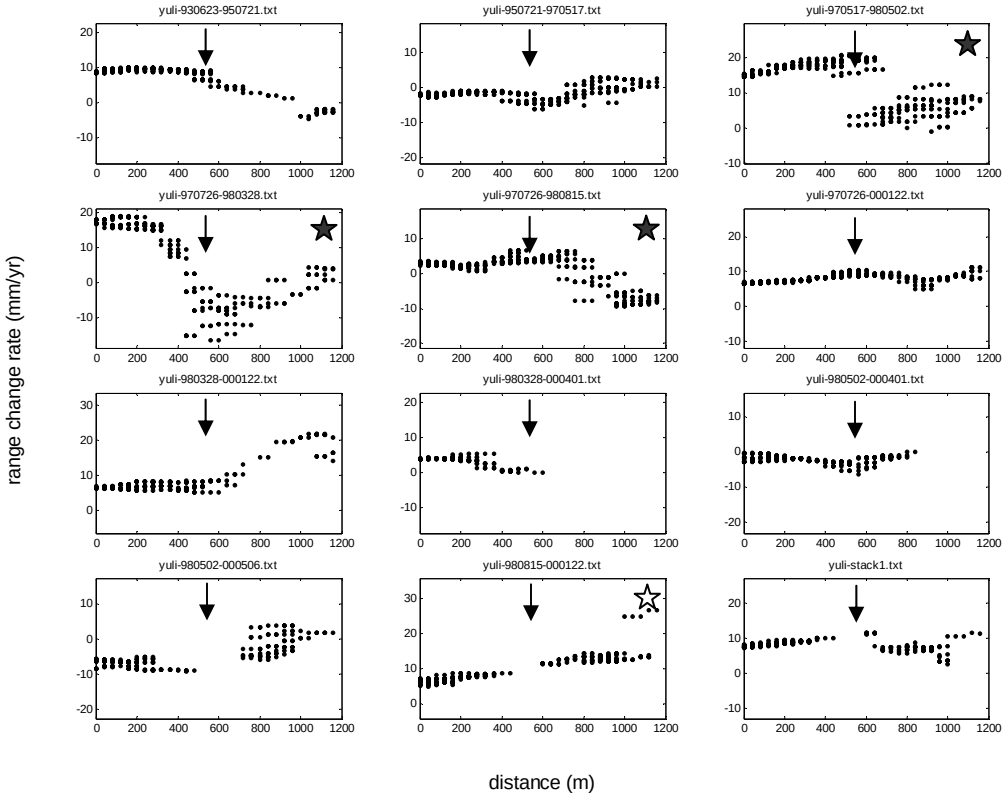

5. Fuli

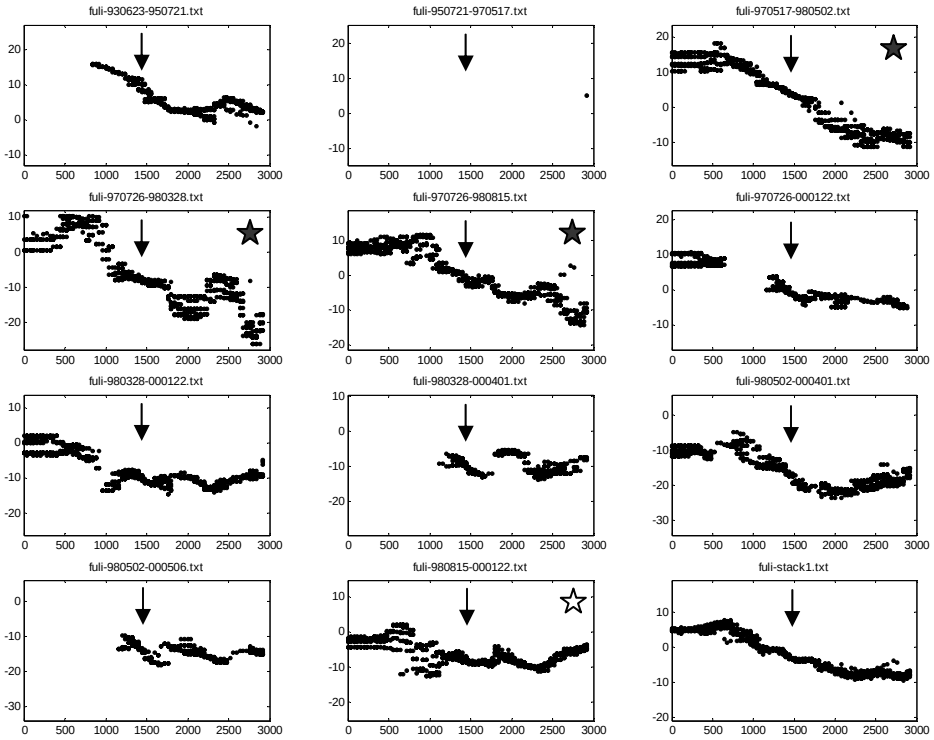

6. Chihshang

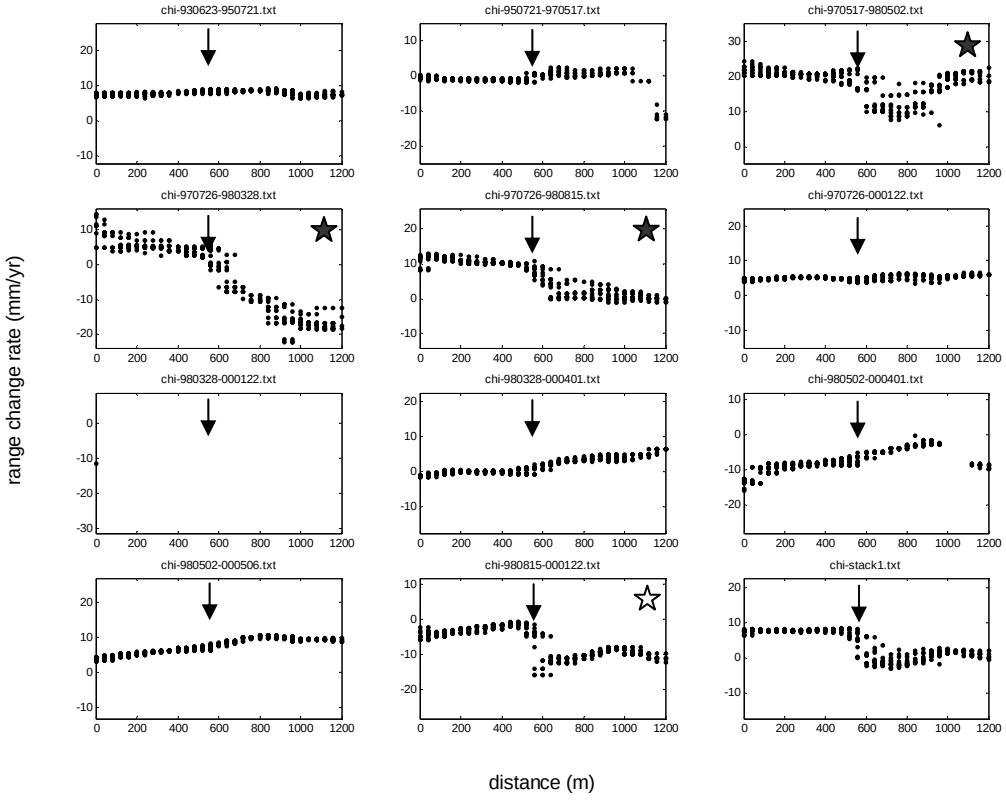

7. Wanan North

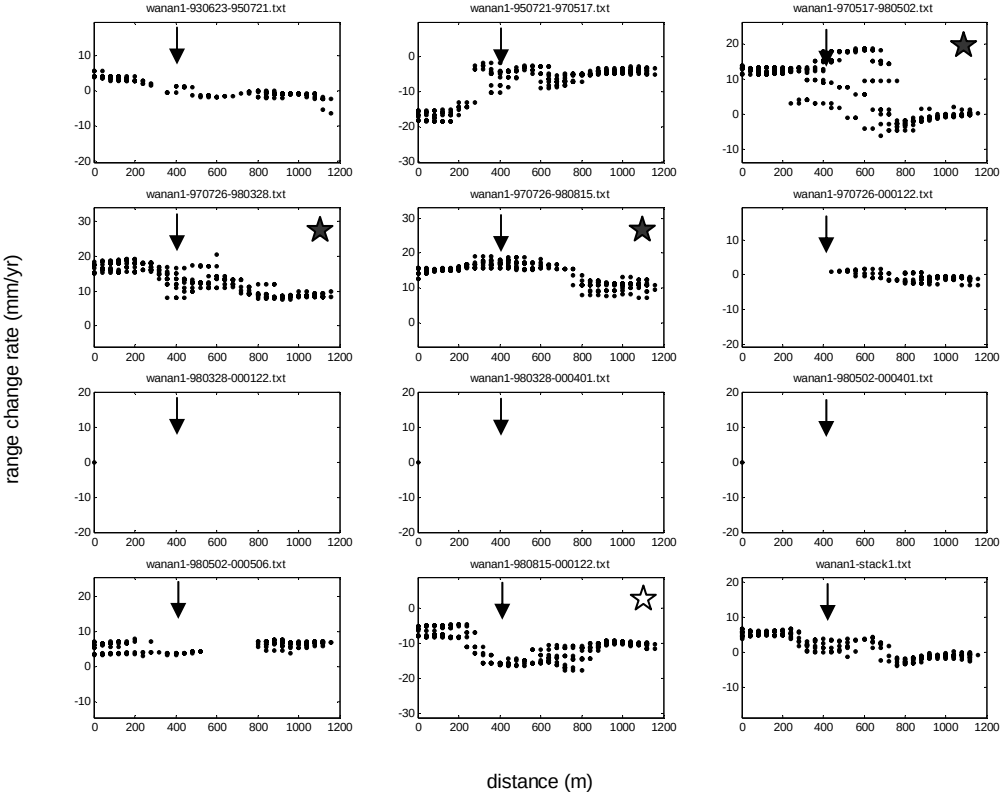

8. Wanan South

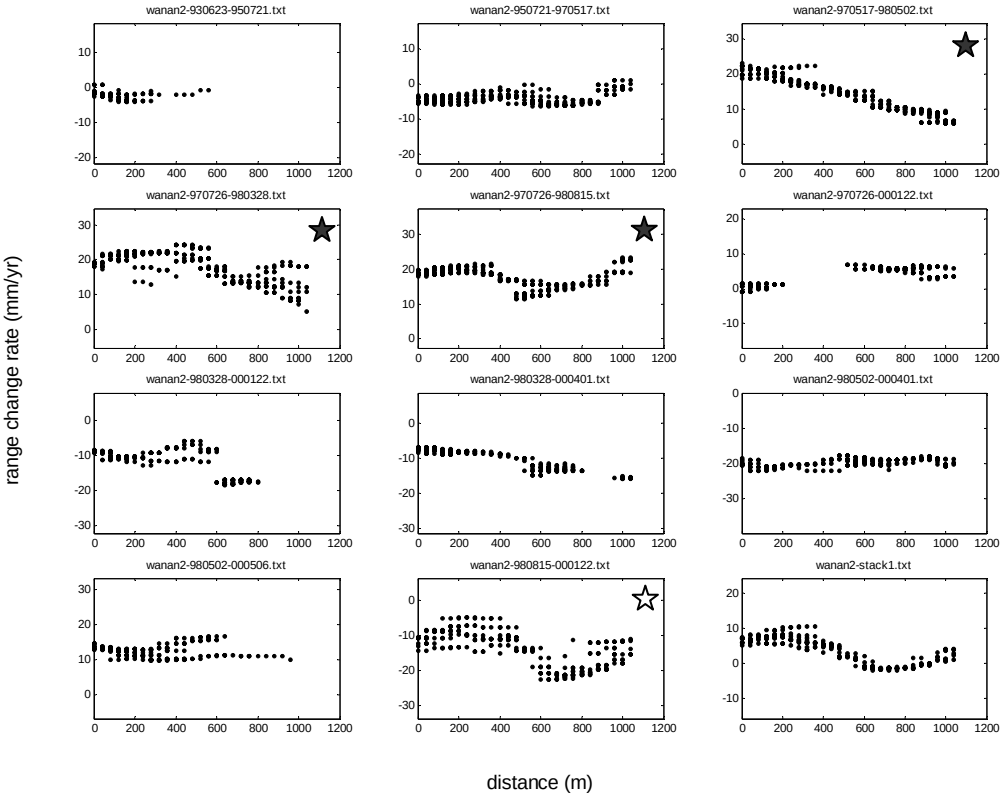

9. Taitung

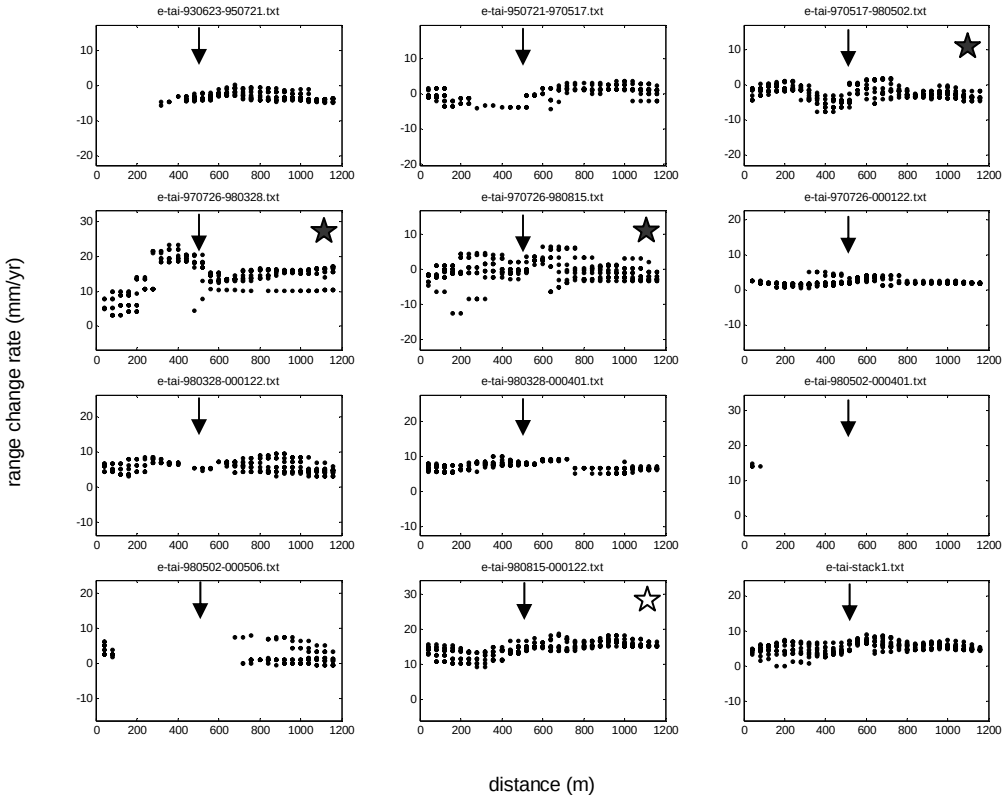

10. Wuhi Tableland

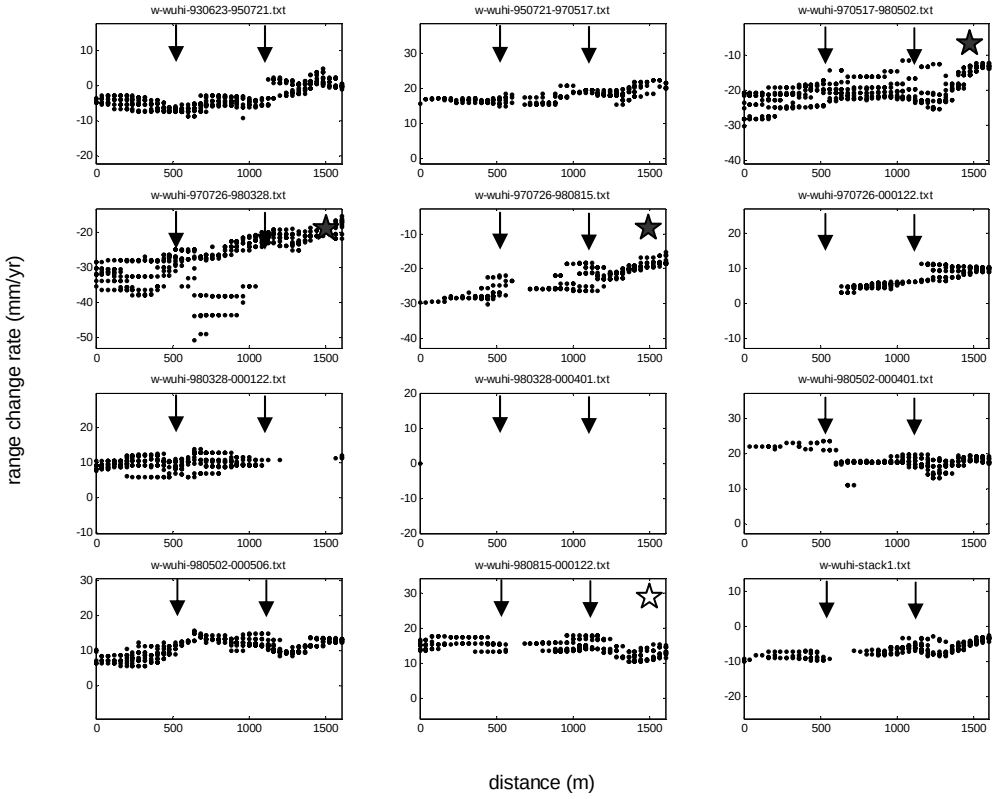

11. W Yuli

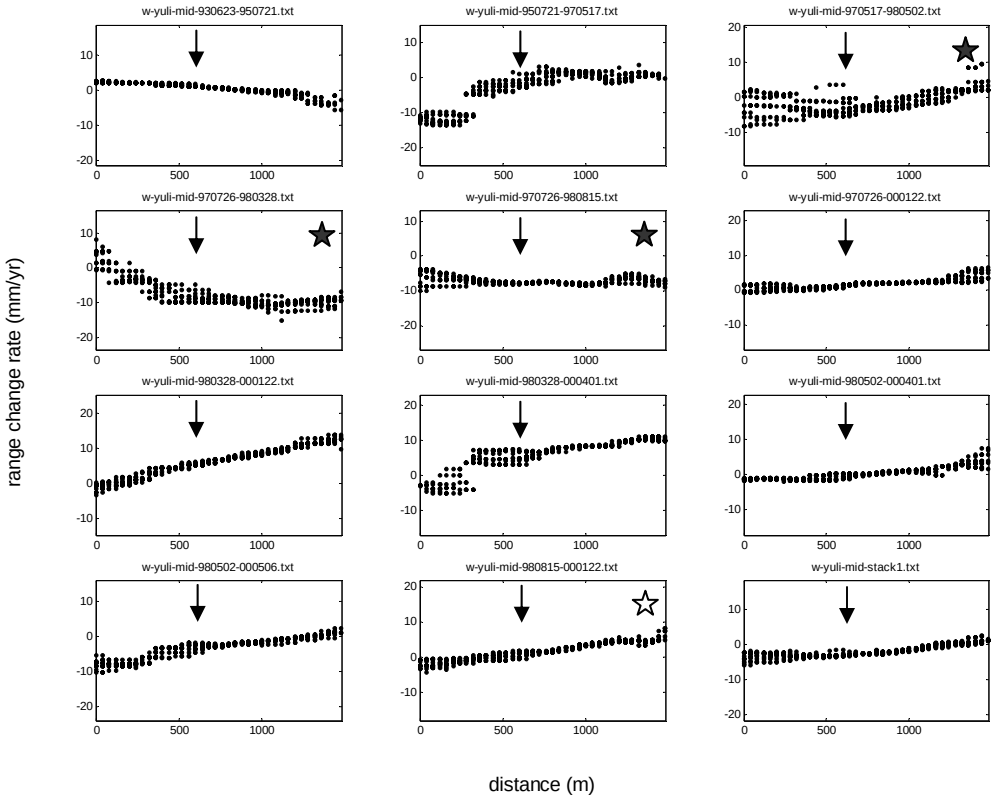

12. Luyeh

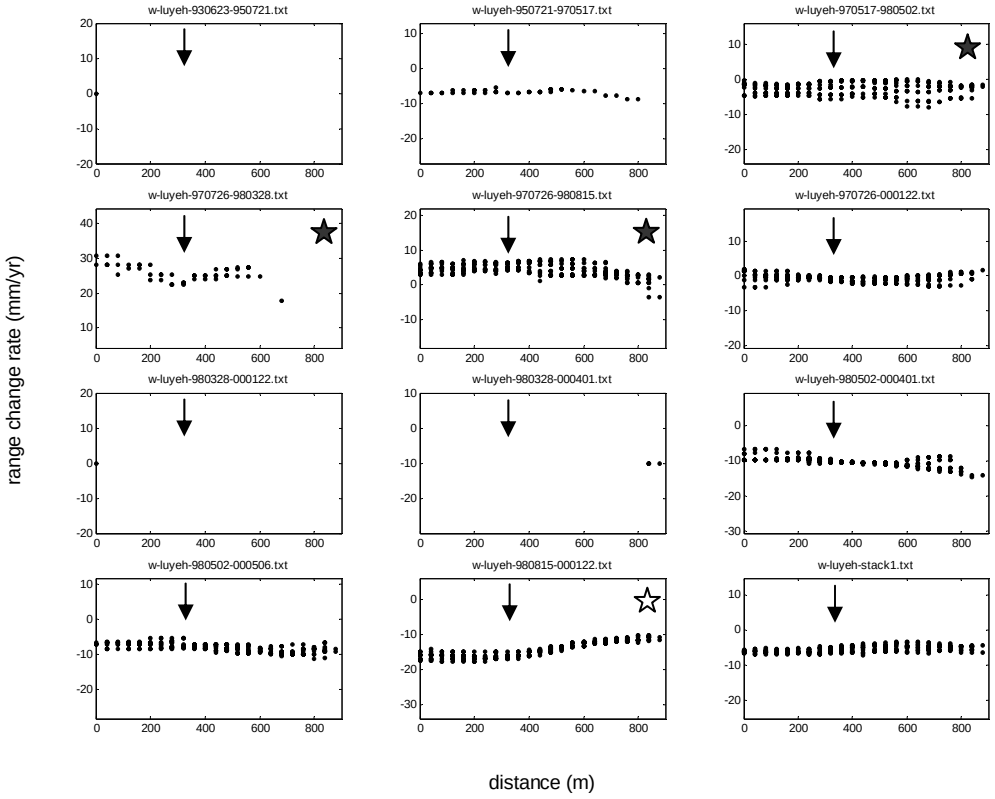

13. W Taitung

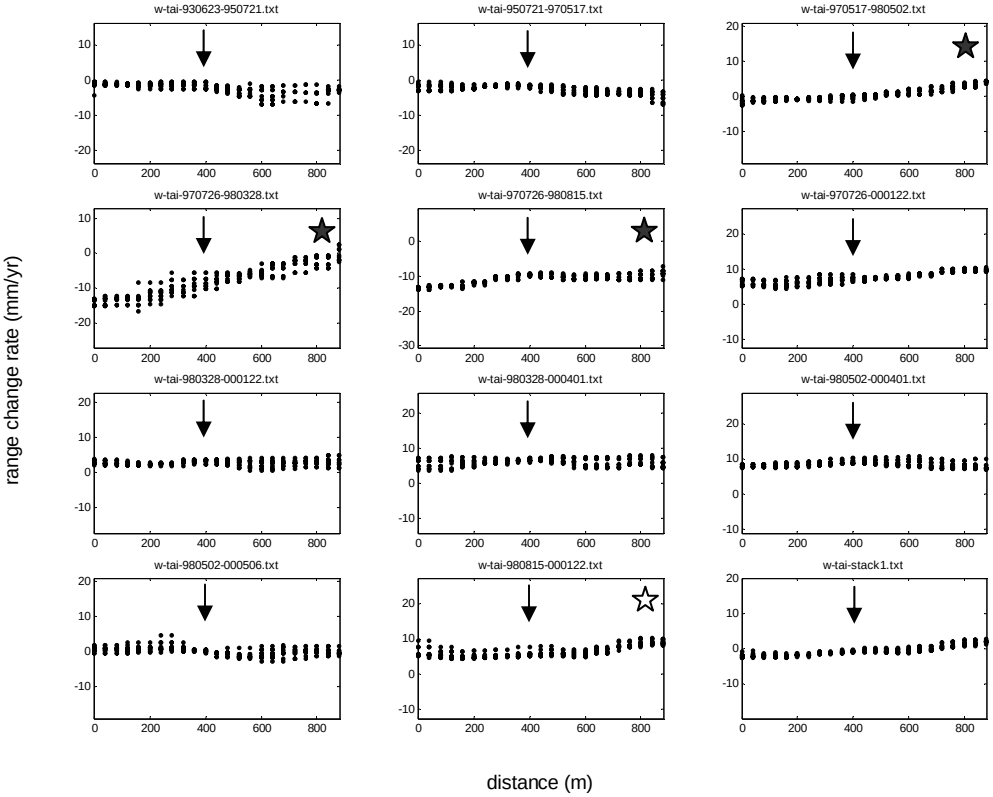

14. W Taitung 2